

# Atmospheric Turbidity Index on Pokhara

Prakash M. Shrestha<sup>1,2</sup>, Suresh Pd. Gupta<sup>1,\*</sup>, Usha Joshi<sup>1,2</sup>, Narayan P. Chapagain<sup>3</sup>, Indra B. Karki<sup>1</sup>, Khem N. Poudyal<sup>4</sup>

<sup>1</sup> Department of Physics, Patan Multiple Campus, TU

<sup>2</sup> Central Department of Physics (CDP), IoST, TU

<sup>3</sup> Department of Physics, Amrit Campus, IoST, TU.

<sup>4</sup> Department of Applied Sciences and Chemical Engineering, Pulchowk Campus, IoE, TU

\* Corresponding e-mail: [suresh.gupta@pmc.tu.edu.np](mailto:suresh.gupta@pmc.tu.edu.np)

Doi : <https://doi.org/10.3126/ppj.v3i01.59036>

## Abstract

*Population growth, industrialization and other natural processes effects on air-pollution levels and climatic change. Atmospheric turbidity factors are an important parameter for assessing the air pollution. The main objective of this research is to study atmospheric turbidity factors on Pokhara (28.18° N, 83.97° E and 800 m asl), Nepal for a period of one year (2017). The daily data of aerosol optical depth (AOD) are derived from Aerosol Robotic Network (AERONET) of NASA. Daily, monthly and seasonal variation of atmospheric turbidity index are analyzed. The annual average of Angstrom exponential ( $\alpha$ ), Angstrom coefficient of turbidity ( $\beta$ ) and Linke turbidity ( $L_T$ ) are found  $1.2 \pm 0.2$ ,  $0.19 \pm 0.17$  and  $6.7 \pm 3.4$  respectively. The annual average of visibility is found  $3.2 \pm 2.5$  km. Result of this research work is beneficial for the further identification, impact and analysis of atmospheric turbidity at different places with same geographical condition.*

**Keywords:** Angstrom exponential, Angstrom coefficient of turbidity, Linke turbidity factor, visibility.

## 1. Introduction

The Sun is closed star from us. The Sun radiates  $4 \times 10^{26}$  W energy in form of electromagnetic wave of wavelength range 300 nm to 3000 nm by thermonuclear fusion reaction [1]. About 1367 W of the solar energy incidents on one square meter area of outer layer of the atmosphere when the Sun and the Earth is energy interacts with components like aerosol, cloud etc. of the atmosphere. The solar energy passing through the atmosphere is scattered and absorbed. According to Beer Lambert's law, the solar energy decreases exponentially in the atmosphere [2]. Aerosols are suspension solid and liquid particle with size  $0.001 \mu\text{m}$  to  $10 \mu\text{m}$ . Both natural and anthropogenic aerosols influence on attenuation of solar energy [3]. The attenuation of solar energy through a real atmosphere verse that through a clean, dry atmosphere gives atmospheric turbidity. Anthropogenic aerosols, black carbon are emitted by vehicles and kilns produces greenhouse effect. Black carbon melts ice on mountain. Particular matter (such as PM1.0, PM2.5, PM10) are responsible for respiratory illness.

Nepal is a land-locked South East Asian mountainous country with a large area of beautiful landscape situated between latitudes of  $26.36^\circ$  N to  $30.45^\circ$  N and longitudes of  $80.06^\circ$  E to  $88.2^\circ$  E. The elevation of the country ranges from 60 m to 8848 m within a span of 200 km from south to north and about 800 km from east to west [4]. In developing

countries like Nepal, the most of energy consumption is fuel wood, agriculture residue, cow dung, coal and petroleum product. There is only 2.4 % [5] of energy consumption is alternative energy line hydroelectricity and solar. Petroleum fuel based vehicle emits huge amount of carbon dioxide and other harmful gases such as Sulphur Dioxide, nitrous oxide, methane, carbon mono oxide etc. Due to the vehicle increase air pollution. Nepal is situated between two giant industrial countries India and China and their industrial byproduct can directly effects concentration of atmospheric components above Nepal. Therefore, detail study of the atmospheric turbidity factors is very important. Its dependence on different meteorological parameters is used in agriculture, Hydrology, Climate change, energy harvesting [6].

**2. Materials and Methods**

The solar energy passing through the atmosphere is scattered and absorbed by components of the atmosphere. The solar radiation decreases in the atmosphere. The opacity of atmosphere for the solar energy gives atmospheric turbidity. There is large number of atmospheric turbidity factors. Angstrom turbidity coefficient ( $\beta$ ), Angstrom exponential ( $\alpha$ ) and Linke turbidity factor ( $L_T$ ) are mostly used [7].

According to angstrom model [8]

$$AOD = \beta \lambda^{-\alpha} \tag{1}$$

Here  $\lambda$  is wavelength. Angstrom exponent ( $\alpha$ ) is an important indicator of the foremost aerosol size [9].  $\alpha$  greater than two indicates small particles associated with combustion byproducts, and values less than one indicates large particles like sea salt and dust.

Linke (1922) proposed to express the total optical thickness of a cloudless atmosphere as the product of two terms, the optical thickness of water and aerosol free atmosphere and the Linke turbidity coefficient ( $L_T$ ) [10]. These atmospheric turbidity factors have been widely used at several places around the world based on solar irradiance measurements to quantify the effects of aerosols and air pollutants on degrading horizontal visibility and reducing the amount of solar radiation reaching the ground. Then, using the Kasten Pyrheliometric formula (1996), the Linke turbidity can be written [11]

$$T_t = (0.4 + 0.9m)(\Delta_{rda} + \Delta_w + \Delta_a) \tag{2}$$

Where m is optical air mass,  $\Delta_{rda}$ ,  $\Delta_w$  and  $\Delta_a$  are optical depth due to Rayleigh scattering, water vapor and aerosol respectively

$$\Delta_{rda} = -0.101 + 0.235m^{0.16}$$

$$\Delta_w = 0.112m^{0.55} w^{0.34}$$

$$\Delta_a = 0.2750 aod_{380} + 0.35 aod_{550}$$

$$m = \frac{P}{101325 \cos \theta_z + 0.15(93.885 - \theta_z)^{-1.253}}$$

Where P is the atmospheric pressure at the place,  $\theta_z$  is solar zenith angle, w is water contained, aod<sub>380</sub> and aod<sub>550</sub> are the aerosol optical depth (AOD) at 380 nm and 550 nm respectively.

Visibility in km is [12]

$$V_{\text{ext}} = \frac{0.673}{b_{\text{ext}}} \quad (3)$$

where  $b_{\text{ext}}$  is AOD at 550 nm.

Daily spectral aerosol optical depth (AOD) data are collected from AERONET website for Pokhara on 2017 for spectral band 675, 500, 440, 380 and 340nm. Open source software Python 3.7 is used to analysis and to plot graph. Mean ( $\bar{x}$ ), standard deviation ( $\sigma$ ), quartiles ( $Q_1$ ,  $Q_2$ ,  $Q_3$ ), skewness ( $\gamma_1$ ) and kurtosis ( $\gamma_2$ ) are used as statistical tools [13]. Standard error (SE) is used as error bar in graph. Data presented in forms of 'mean  $\pm$  standard deviation'.

Pokhara ( $28.18^\circ$  N,  $83.97^\circ$  E and 800 m asl) lies in Kaski district of Gandaki Province as shown in Figure 1. Pokhara is capital of Gandaki Province and headquarter of Kaski district. Pokhara is the city of lakes ( like Phewa, Begnas, Rupa ). Three peaks Dhaulagiri, Annapurna, Manaslu with more than 8000~m height can be seen from the city. The Machhapuchhre (Fishtail) with an elevation of 6,993 metres is the closest to the city. Pokhara covers 464.24 sq. km. and 4.4 sq.km water. It has population 599,504 and population density is 1,300 per sq.km [14]. The average temperatures is between  $25$  and  $35^\circ$  C in summer and  $-2$  to  $15^\circ$  C in winter. Pokhara receives a high amount of precipitation in the country 3,350 mm/year. Yearly mean daily solar radiation is  $16.499$  MJ/m<sup>2</sup>/day from 2007 to 2012 in Pokhara [15]. The maximum solar radiation is  $23.21$  MJ/m<sup>2</sup>/day in June and minimum is  $12.04$  MJ/m<sup>2</sup>/day in December from 2009 to 2010 in Pokhara [16].



**Figure 1:** Map of Pokhara [source: Department of survey, Gov. of Nepal, 2020]

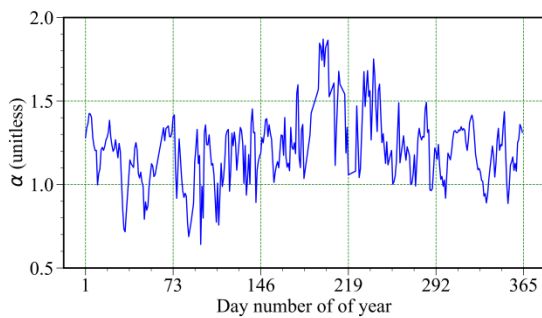


### 3. Results and Discussion

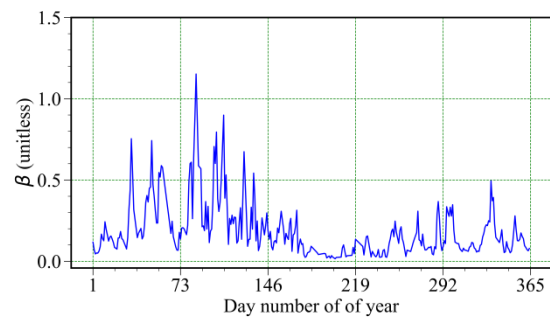
Daily data of spectral aerosol optical depth (AOD) are downloaded from AERONET website for Pokhara on 2017. By using wavelength ( $\lambda$ ) of 675, 500, 440, 380 and 340 nm and aerosol optical depth (AOD), daily data of Angstrom exponential ( $\alpha$ ) and Angstrom coefficient of turbidity ( $\beta$ ) are calculated by linear regression method for equation (1). Daily data of Linke turbidity factor ( $L_T$ ) and visibility are calculated by using equation (1), (2) and (3) respectively.

Figure 2 and 3 show respectively daily variation and corresponding histogram of  $\alpha$ ,  $\beta$ ,  $L_T$  and visibility. Figure 2(a) and 3(a) show respectively daily variation and histogram of

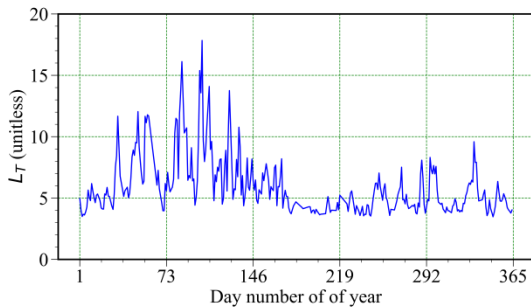
$\alpha$ . During study period of 2017, the maximum value of  $\alpha$  is found 1.8 on July 18. As  $\alpha$  is less than one, atmosphere of that day contains large aerosol. The minimum value of  $\alpha$  is 0.6 on April 7. As  $\alpha$  is greater than one, atmosphere of that day contains fine mode aerosol. The annual mean and standard deviation are found 1.2 and 0.2 respectively. The first quartile ( $Q_1$ ), second quartile ( $Q_2$ , median) and third quartile ( $Q_3$ ) are found 1.1, 1.2 and 1.3 respectively. Skewness ( $\gamma_1$ ) and the kurtosis ( $\gamma_2$ ) are found 0.38 and 0.91 respectively. The distribution of  $\alpha$  is positively tailed and is not Gaussian. Out of 313 study days, 142 days has  $\alpha$  between 1.2 to 1.5. Figure 2(b) and 3(b) show respectively daily variation and histogram of  $\beta$ . During study period, the maximum value of  $\beta$  is found  $\beta$  is 0.01 on July 22, atmosphere of that day is clear. The annual mean and standard deviation are found 0.19 and 0.17 respectively. The first quartile ( $Q_1$ ), second quartile ( $Q_2$ , median) and third quartile ( $Q_3$ ) are found 0.08, 0.13 and 0.23 respectively. Skewness ( $\gamma_1$ ) and kurtosis ( $\gamma_2$ ) are found 2.11 and 5.51 respectively. The distribution of  $\beta$  is positively tailed and is not Gaussian. Out of 313 study days, 215 days has  $\beta$  between 0 to 0.2.



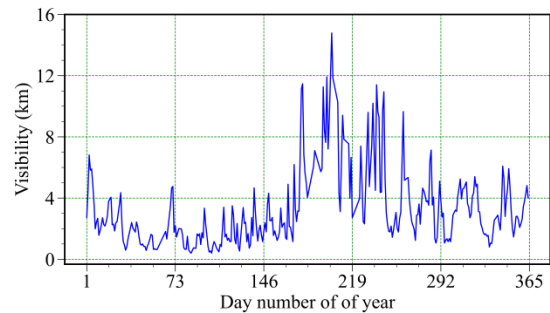
a) Daily variation of  $\alpha$



b) Daily variation of  $\beta$



c) Daily variation of  $L_T$

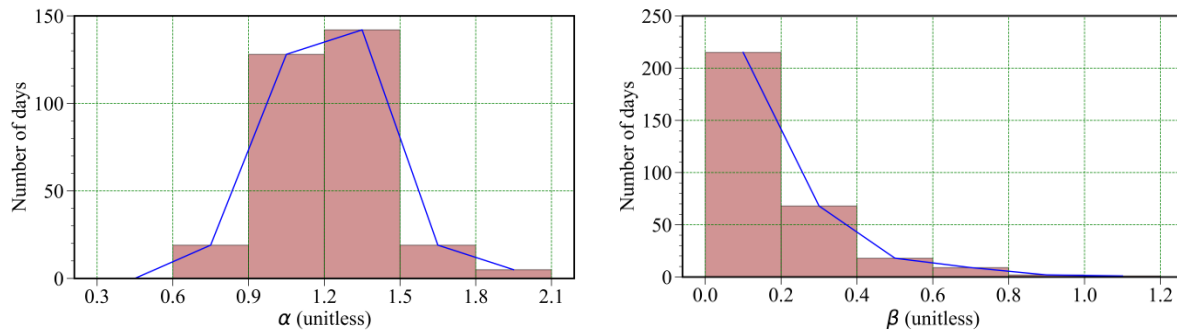


d) Daily variation of visibility

**Figure.2:** Daily Variation of Angstrom exponential ( $\alpha$ ), Angstrom coefficient of turbidity ( $\beta$ ), Linke turbidity factor ( $L_T$ ) and visibility

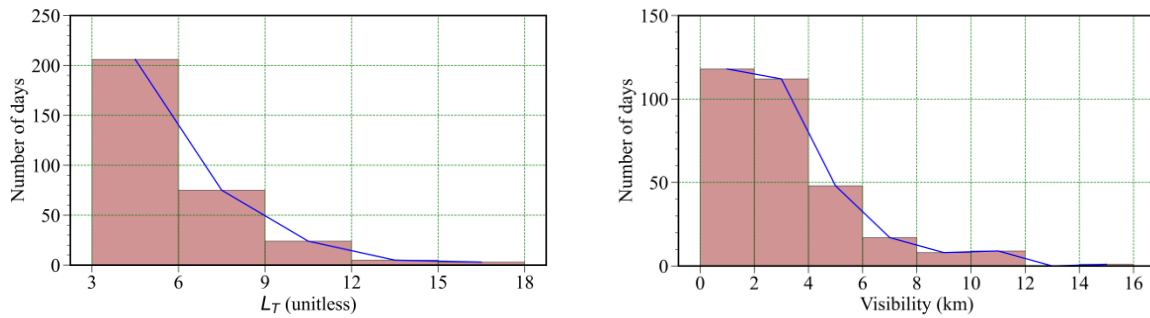
Figure 2(c) and 3(c) show respectively daily variation and histogram of  $L_T$ . During study period, the maximum value of  $L_T$  is found 17.8 on April 24, atmosphere of that day highly polluted. The minimum value of  $L_T$  is 3.4 on September 6, atmosphere of that day is clear. The annual mean and standard deviation are found 0.19 and 0.17 respectively. The first

quartile ( $Q_1$ ), second quartile ( $Q_2$ , median) and third quartile ( $Q_3$ ) are found 4.2, 5.2 and 6.6 respectively. Skewness ( $\gamma_1$ ) and kurtosis ( $\gamma_2$ ) are found 1.90 and 4.32 respectively. The distribution of  $L_T$  is positively tailed and is not Gaussian. Out of 313 study days, 206 days has  $L_T$  between 3 to 6. Figure 2(d) and 3(d) show respectively daily variation and histogram of visibility. During study period, the maximum value of visibility is found 15 km on July 22. The minimum value of visibility is 0.4 km on March 28. The annual mean and standard deviation are found 3.2 km and 2.5 km respectively. The first quartile ( $Q_1$ ), second quartile ( $Q_2$ , median) and third quartile ( $Q_3$ ) are found 1.5, 2.4 and 4.1 respectively. Skewness ( $\gamma_1$ ) and kurtosis ( $\gamma_2$ ) are found 1.73 and 3.28 respectively. The distribution of visibility is positively tailed and is not Gaussian. Out of 313 study days, 118 days has visibility between 0 to 2 km.



a) Histogram of  $\alpha$

b) Histogram of  $\beta$



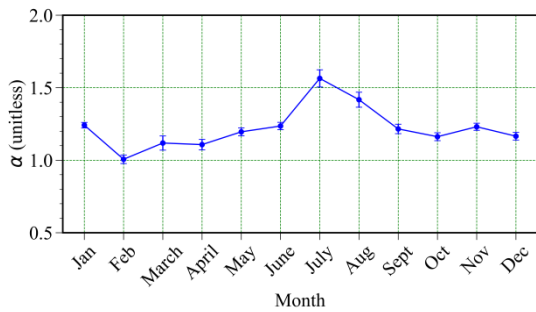
c) Histogram of  $L_T$

d) Histogram of visibility

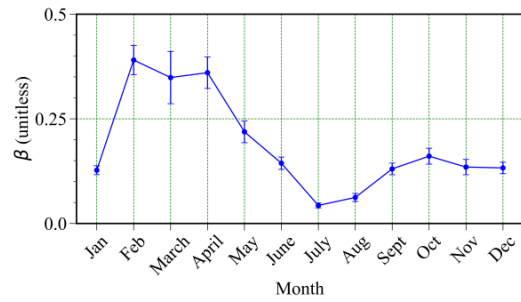
**Figure.3:** histogram of Angstrom exponential ( $\alpha$ ), Angstrom coefficient of turbidity ( $\beta$ ), Linke turbidity factor ( $L_T$ ) and visibility

Figure 4 show monthly variation of  $\alpha$ ,  $\beta$ ,  $L_T$  and visibility. Figure 4(a) shows monthly variation of  $\alpha$ . During study period of one year 2017, the maximum and minimum value of month average of  $\alpha$  is found  $1.5 \pm 0.2$  in July and  $1.0 \pm 0.1$  in February respectively. Variation is large in March due to large standard deviation and is less in January due to small stan

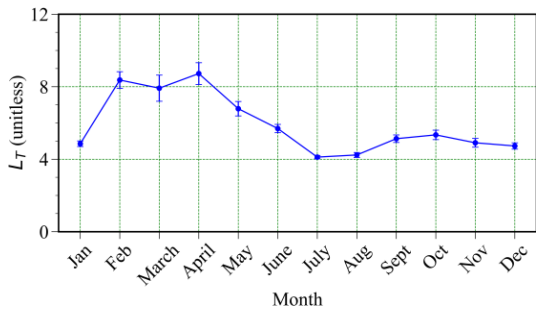
dard deviation. Figure 4(b) shows monthly variation of  $\beta$ . During study period of one year 2017, the maximum and minimum value of month average of  $\beta$  are found  $0.49 \pm 0.17$  in February and  $0.06 \pm 0.04$  in July respectively. Variation is large in March due to large standard deviation and is less in July due to small standard deviation. Figure 4(c) show monthly variation of  $L_T$ . During study period of one year 2017, the maximum and minimum value of month average of  $L_T$  are found  $8.7 \pm 3.1$  in April and  $4.1 \pm 0.4$  in July respectively. Variation is large in March due to large standard deviation and is less in July due to small standard deviation. Figure 4(d) shows monthly variation of visibility. During study period of one year 2017, the maximum and minimum value of month average of visibility are found  $7.9 \pm 3.1$  km in July and  $1.2 \pm 0.5$  km in February respectively. Variation is large in July due to large standard deviation and is less in February due to small standard deviation.



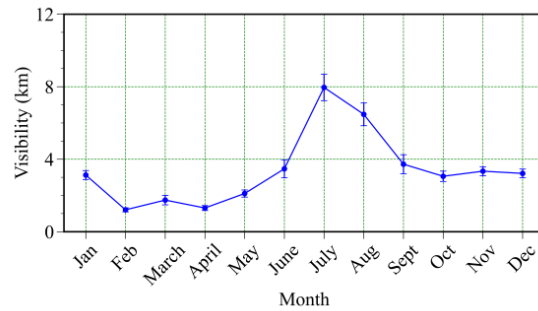
a) Monthly variation of  $\alpha$



b) Monthly variation of  $\beta$



c) Monthly variation of  $L_T$



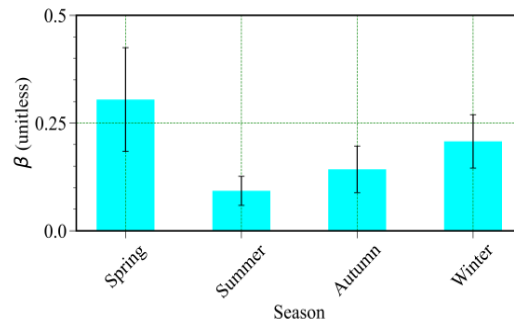
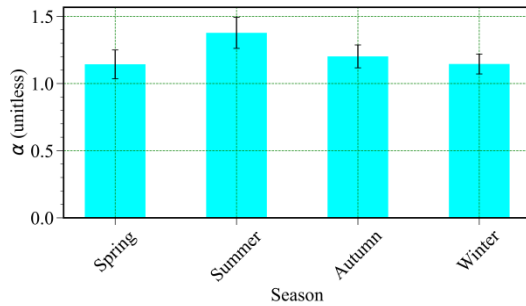
d) Monthly variation of visibility

**Figure.4:** Monthly variation of Angstrom exponential ( $\alpha$ ), Angstrom coefficient of turbidity ( $\beta$ ),

*Linke turbidity factor ( $L_T$ ) and visibility*

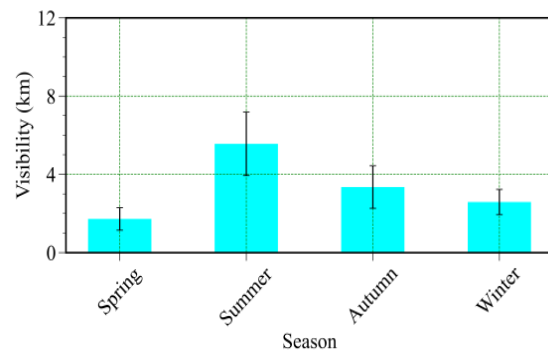
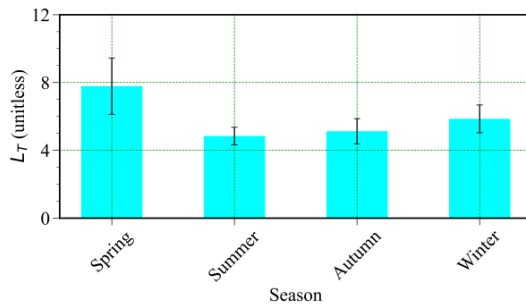
Figure 5 show seasonal variation of  $\alpha$ ,  $\beta$ ,  $L_T$  and visibility. Figure 4(a) shows seasonal variation of  $\alpha$ . During study period of one year 2017, the maximum and minimum value of average of  $\alpha$  is found  $1.4 \pm 0.2$  in summer and  $1.1 \pm 0.2$  in spring respectively. Variation is large in summer due to large standard deviation and is less in winter due to small standard

deviation. Figure 4(b) shows seasonal variation of  $\beta$ . During study period of one year 2017, the maximum and the minimum value of average of  $\beta$  are found  $0.30 \pm 0.20$  in spring and  $0.09 \pm 0.05$  in summer respectively. Variation is large in spring due to large standard deviation and is less in summer due to small standard deviation. Figure 4(c) shows seasonal variation of  $L_T$ . During study period, the maximum and minimum value of average of  $L_T$  is found  $7.8 \pm 2.9$  in spring and  $4.8 \pm 0.9$  in summer respectively. Variation is large in spring due to large standard deviation and is less in summer due to small standard deviation. Figure 4(d) shows seasonal variation of visibility. During study period, the maximum and minimum value of average of visibility are found  $5.5 \pm 2.8$  km in summer and  $1.7 \pm 1.0$  km in spring respectively. The variation is large in summer due to large standard deviation and is less in spring due to small standard deviation.



a) Seasonal variation of  $\alpha$

b) Seasonal variation of  $\beta$



c) Seasonal variation of  $L_T$

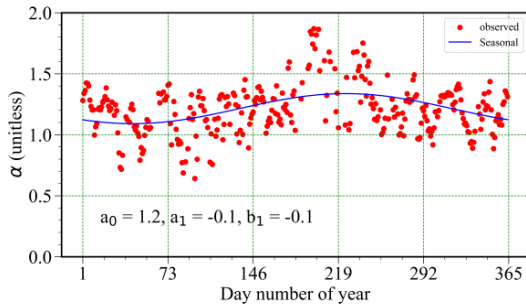
d) Seasonal variation of visibility

**Figure.5:** Seasonal variation of Angstrom exponential ( $\alpha$ ), Angstrom coefficient of turbidity ( $\beta$ ), Linke turbidity factor ( $L_T$ ) and visibility

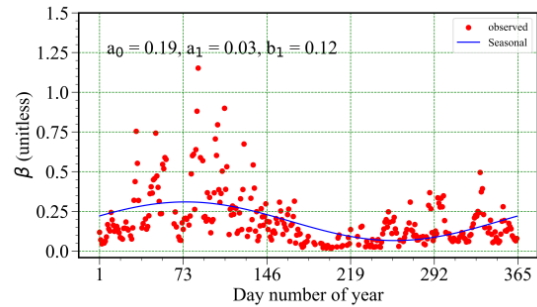
Fourier series is used to analysis season variation of time series data [17].

$$y_s = a_0 + a_1 \cos\left(\frac{2\pi}{365}n_d\right) + b_1 \sin\left(\frac{2\pi}{365}n_d\right) \quad (4)$$

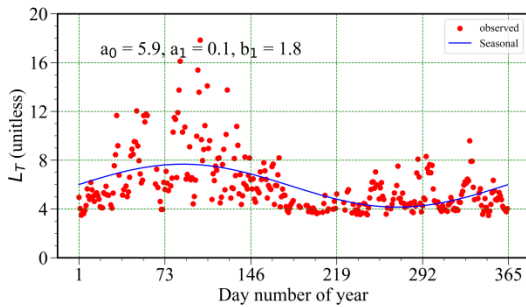
Here  $n_d$  is day number of year (DOY),  $a_0$  and  $\sqrt{a_1^2 + b_1^2}$  are offset and amplitude of seasonal components respectively. Figure 6 show Fourier analysis of  $\alpha$ ,  $\beta$ ,  $L_T$  and visibility. In figure 6(a), offset and amplitude of seasonal components of  $\alpha$  are 1.2 and 0.1 respectively. In figure 6(b), offset and amplitude of seasonal components of  $\beta$  are 0.19 and 0.12 respectively. In figure 6(c), offset and amplitude of seasonal components of  $L_T$  are 5.9 and 1.7 respectively. In figure 6(d), offset and amplitude of seasonal components of visibility are 3.3 km and 1.9 km respectively.



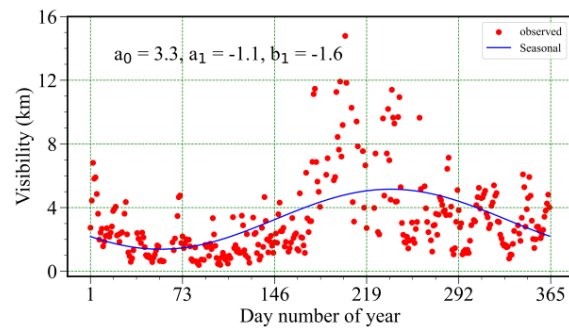
a) Fourier analysis of  $\alpha$



b) Fourier analysis of  $\beta$



c) Fourier analysis of  $L_T$



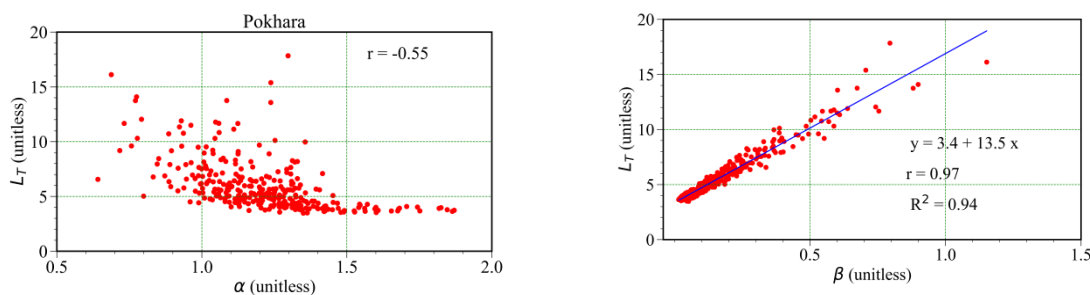
d) Fourier analysis of visibility

**Figure.6:** Fourier analysis of Angstrom exponential ( $\alpha$ ), Angstrom coefficient of turbidity ( $\beta$ ), Linke turbidity factor ( $L_T$ ) and visibility

Figure 7 show relation between  $\alpha$ ,  $\beta$  with  $L_T$ . Figure 7(a) shows relation between  $\alpha$  with  $L_T$ . The correlation coefficient ( $r$ ) between  $\alpha$  and  $L_T$  is -0.55. They are negatively correlated with moderate value. Figure 7(b) shows relation between  $\beta$  with  $L_T$ . The correlation coefficient between  $\beta$  and  $L_T$  is 0.97. They are positively correlated with high value. They are fitted in straight line ( $y = mx + c$ ) by least square method. The straight line obtained is

$$L_T = 3.4 + 13.5\beta$$

The straight line is fitted with 94% of coefficient of determination ( $R^2$ ).

a) Relation between  $\alpha$  with  $L_T$ b) Relation between  $\beta$  with  $L_T$ **Figure.7:** Relation between  $\alpha$ ,  $\beta$  with  $L_T$ 

#### 4. Conclusion

Datasets on atmospheric turbidity is of great importance to the detection of global warming and climate change. The atmospheric turbidity factors calculated from AERONET network data on basis of atmospheric turbidity model is therefore important to propose solar radiation potential of the location, the sustainable development of ecological environments and agriculture based productivity. In study period of one year (2017), the annual mean of Angstrom exponential ( $\alpha$ ), Angstrom coefficient of turbidity ( $\beta$ ) and Linke turbidity ( $L_T$ ) are found  $1.2 \pm 0.2$ ,  $0.19 \pm 0.17$  and  $6.7 \pm 3.4$  respectively. The annual average of visibility is found  $3.2 \pm 2.5$  km. Angstrom turbidity coefficient ( $\beta$ ) in Kathmandu on 1999 are  $0.6247 \pm 0.023$  and  $0.2997 \pm 0.009$  respectively [18]. Linke turbidity is  $1.97 \pm 0.47$  on Jumla on 2012 [19]. Linke turbidity is  $5.53 \pm 0.23$  on Kathmandu Valley on 2012 [20]. Linke turbidity is  $5.7 \pm 2.5$  on Bode, Bhaktpur on 2013 [21]. The annual average of Linke turbidity index ( $L_T$ ) and visibility are  $2.5 \pm 1.1$  and  $10.4 \pm 3.8$  km respectively on over Deukhuri Valley, Dang period of 4 years (2015, 2016, 2017, 2018) [22]. Linke turbidity is 3.3 to 7.7 in Wuhan, Central China from 2010 to 2011 [23]. On eight years (1993 to 2000) study, Linke turbidity for four cities of India are 7.5 for Kolkata, 4.6 for Poona, 6.4 for Jaipur and 6.8 for New Delhi [24]. At Qena, Egypt, Linke turbidity index was  $5.5 \pm 0.26$  in hot season and was  $4.45 \pm 0.44$  in cold season from 2001 to 2004 [25]. A comparison of observed values of turbidity parameter with other major cities of the world shows that Pokhara is not polluted as cities like New Delhi, Qena, Kolkota, Jaipur etc.

#### Acknowledgment

Authors are grateful to express thank to faculty members of Central Department of Physics (CDP), Department of Physics of Patan Multiple Campus, Institute of Science and Technology (IoST). Authors are highly acknowledged to NASA for data and Nepal Academy of Science and Technology (NAST) for providing PhD fellowship. We also like to acknowledge Nepal Physical Society (NPS) and Association of Nepali Physicists in America (ANPA) for educational workshop of Python.

**References**

- [1] Khem N Poudyal, Binod K Bhattarai, Balkrishna Sapkota, and Berit Kjeldstad(2011). Solar radiation potential at four sites of Nepal. *Journal of the Institute of Engineering*, 8(3):189–197.
- [2] GF Lothian. Beer's law and its use in analysis(1953). a review. *Analyst*, 88(1050):678–685.
- [3] Veerabhadran Ramanathan and Gregory Carmichael(2008). Global and regional climate changes due to black carbon. *Nature geoscience*, 1(4):221–227.
- [4] Majupuria R K Majupuria T C(1999). *Nepal nature's paradise: insight into diverse facets of topography, flora and ecology*. M Devi, Gwalior,India.
- [5] MoF. *Economic Survey 2021/022(2022)*. Ministry of Finance, Government of Nepal.
- [6] Khem N Poudyal, Binod K Bhattarai, Balkrishna Sapkota, Berit Kjeldstad, and Pasquale Daponte (2013). Estimation of the daily global solar radiation; nepal experience. *Measurement*, 46(6):1807–1817.
- [7] Yousef A Eltbaakh, Mohd Hafidz Ruslan, MA Alghoul, Mohd Yusof Othman, and Kamaruzzaman Sopian(2012). Issues concerning atmospheric turbidity indices. *Renewable and Sustainable Energy Reviews*, 16(8):6285–6294.
- [8] Anders Angstrom(1951). Techniques of determinig the turbidity of the atmosphere. *Tellus*, 13(2):214–223.
- [9] Gregory L Schuster, Oleg Dubovik, and Brent N Holben(2006). Angstrom exponent and bimodal aerosol size distributions. *Journal of Geophysical Research: Atmospheres*, 111(D7).
- [10] Pierre Ineichen and Richard Perez(2002). A new airmass independent formulation for the linke turbidity coefficient. *Solar Energy*, 73(3):151–157.
- [11] Pierre Ineichen(2008). Conversion function between the linke turbidity and the atmospheric water vapor and aerosol content. *Solar Energy*, 82(11):1095–1097.
- [12] Harald Koschmieder(1924). Theorie der horizontalen sichtweite. *Beitrage zur Physik der freien Atmosphere*, pages 33–53.
- [13] Larry J. Stephens Murray R. Spiegel(1998). *Schaum's Outline of Theory and Problems of Statistics (Schaum's Outline Series)*. McGraw-Hill.
- [14] CBS. *National Population and Housing Census 2021(2023)*. Central Bureau of Statistics, National Planning Commission Secretariat, Government of Nepal.
- [15] Krishna R Adhikari, Binod K Bhattarai, and Shekhar Gurung(2013). Solar energy potential in nepal and global context. *Journal of the Institute of Engineering*, 9(1):96 – 106.
- [16] Khem N Poudyal(2015). Estimation of global solar radiation using modified angstrom empirical formula on the basis of meterological parameters in himalaya region pokhara, nepal. *Journal of the Institute of Engineering*, 11(1):158–164.

- [17] Manuel Anton, Daniele Bortoli, Maria Joao Costa, PS Kulkarni, Ana Filipa Domingues, David Barriopedro, Antonio Serrano, and Ana Maria Silva(2011). Temporal and spatial variabilities of total ozone column over portugal. *Remote Sensing of Environment*, 115(3):855–863.
- [18] B Sapkota and Rajan Dhaubhadel(2002). Atmospheric turbidity over kathmandu valley. *Atmospheric Environment*, 36(8):1249–1257.
- [19] Prakash M Shrestha, Indra B Karki, Narayan P Chapagain, and Khem N Poudyal(2019). Study of linke turbidity factor on solar radiation over jumla. *Molung Educational Frontier*, 9:141–149.
- [20] Prakash M. Shrestha, Khem N. Poudyal, Narayan P. Chapagain, and Indra B. Karki(2020). Study of impact of linke turbidity on solar radiation over kathmandu valley. *Patan Pragya*, 6(1):191–198.
- [21] Prakash M Shrestha, NP Chapagain, IB Karki, and KN Poudyal(2020). Study of linke turbidity factor over bode, bhaktapur. *Journal of Nepal Physical Society*, 6(2):66–73.
- [22] Prakash M Shrestha, SP Gupta, U Joshi, NP Chapagain, IB Karki, and KN Poudyal(2022). Atmospheric linke turbidity index over deukhuri valley, dang. *Journal of Nepal Physical Society*, 8(2):1–6.
- [23] Lunche Wang, Yisen Chen, Ying Niu, Germán Ariel Salazar, and Wei Gong(2017). Analysis of atmospheric turbidity in clear skies at wuhan, central china. *Journal of Earth Science*, 28(4):729–738.
- [24] Laxmi Narain and SN Garg(2013). Estimation of linke turbidity factors for different regions of india. *International Journal of Environment and Waste Management*, 12(1):52–64.
- [25] M El-Nouby Adam and Eman F El-Nobi(2017). Correlation between air temperature and atmospheric turbidity at a subtropical location. *World Environment*, 7(1):1–9.